CHAPTER 3

Calibration Errors

I .this Chapter, we discuss the various sources of errors in the measurement of absolute flux and present observations for estimating these errors.

The r.m.s. noise on a spectrum is given by the usual formula:

$$\sigma = \frac{\alpha T}{\sqrt{B\tau}} \qquad (1)$$

where the constant a is 2 for position/beam switching, and $\sqrt{2}$ for frequency-switched data (after folding). Leaving out these fluctuations due to system noise, the possible causes for an error in the absolute flux, are listed below.

3.1 Causes of error in gain calibration

- **Pointing.** The residual pointing errors are discussed in the earlier section on pointing calibration. The main beam of the 10.4 m telescope at 86 GHz, is approximately a gaussian with a width (FWHM) of 70". We shall call a source point-like if its angular size is much less than this. For a point-like source, a fractional decrease in the measured flux by 20% can be caused by a radial[1] pointing error of 20", while an error of 10" leads to a 5% loss. From the rms values of residual pointing errors found from continuum scans on planets, we estimate the maximum loss in flux due to them, to be about 10 to 15% during 1988 and 1989 and about 20% during 1990.

- **Switching problems.**

  1. If the chopper wheel does not fully return to the sky position after the cal run, the subsequent data will be affected.

[1] $(\Delta A)^2 + (\Delta E)^2$

2. Loss in the signal strength can also be caused by improper switching of the mirror. However, the status of the mirror/chopper operation is monitored remotely at the control panel during observations, so that an error due to these factors is unlikely.

3. In the frequency switching mode, if the synthesizer frequency drifts within a small enough range, the PLL may still remain locked but the spectral line will get 'smeared' resulting in a smaller value of the antenna temperature (though the integrated flux may remain the same). The frequency of the synthesizer is also monitored at the control panel and data is not acquired when frequency drifts occurred.

- Day time heating up of the dish and consequent distortions can lead to poorer efficiency.

- Due to gravitational flexure etc., the efficiency of the dish can become elevation dependent.

- **Bad sky.**

1. Clouds, either smaller than beam-throw size, or fast moving, can cause errors.

2. Differences in the sky at times of mirror switched acquisition and the chopper acquisition.

To estimate the error in measured flux, we have the following data:

1. Continuum scans taken on planets.

2. Spectral-line observations (SiO maser at 86 GHz) of Orion taken during the regular observations of Mira variables.

3. Spectral-line observations of R Cas made on 6th March 1990, every few minutes for a time interval of about 2 hours.

Each of these data-sets gives us the following information regarding errors in absolute flux measurements.

From the scans taken on planets, we obtain the pointing offsets and aperture efficiency (as described earlier). The spectral-line observations of Orion were made with the motivation of checking the consistency of these telescope parameters during the regular observations, However, as we shall see, Orion is probably not a suitable calibration source due to its time-variation over a time-scale of few days. The observation of R Cas was done over a period of 2 hrs, during which the telescope error in pointing, and the aperture efficiency remain constant as these are slowly varying functions of azimuth and elevation. Therefore from this run on R Cas, we can estimate the repeatability of the chopper-wheel calibration to correct for the atmospheric attenuation.

We shall now discuss each of these three sets individually, starting with spectral-line observations.

3.2 Check runs on Orion

The variation in the intensity of spectral-lines from Orion, may be due to the following reasons:

1. Calibration error: including pointing error since the measurements are made at different times and angular positions on the sky.

2. Inherent time variations in the source.

3. Polarization parallactic angle variations due to our having an altitude-azimuth mount, a single linearly polarized feed and observations being at different hour angles.

There are three main features in the spectral line from Orion. Consider the 1^{st} and the 3^{rd} features which are stronger (see Fig. 1). The ratio of the strengths of these peaks is independent of instrumental errors. This ratio is plotted in Fig. 7. It is interesting to note that a relative time-variation of features within the profile is seen. We shall return to this later in Chapter 7.

Table 1 lists the parameters obtained from fitting gaussians to these line-profiles. The rms errors on these parameters are related to the residual rms of the fit as follows (Rieu, 1969).

$$\sigma_A = \left(\frac{\Delta V_o}{\Delta V}\right)^{\frac{1}{2}} \sigma \tag{2}$$

$$\sigma_{\Delta V} = 1.16\,(\Delta V_o \Delta V)^{\frac{1}{2}}\,\frac{\sigma}{T} \tag{3}$$

$$\sigma_V = 0.49\,(\Delta V_o \Delta V)^{\frac{1}{2}}\,\frac{\sigma}{T} \tag{4}$$

In these formulae, a is the residual rms of the gaussian fit (whenever this quantity was found to be smaller than that due to the noise, we have used the latter value). T is the fitted peak antenna temperature, AV is the fitted width and ΔV_o is the instrumental velocity resolution.

In Table 1, the velocities of numbers 6 and 11, are off by 1 km/s, due to an error in the calibration of the AOS. The observations made on these days have been corrected for this error. The parameters in Table 1 are plotted against Julian day number in Fig. 2—4. The 1988 data is plotted again on a scale expanded in the x-axis. Figs. 5 shows that during the 1988 observing season, there appears to be a fractional variation on the integrated antenna temperature

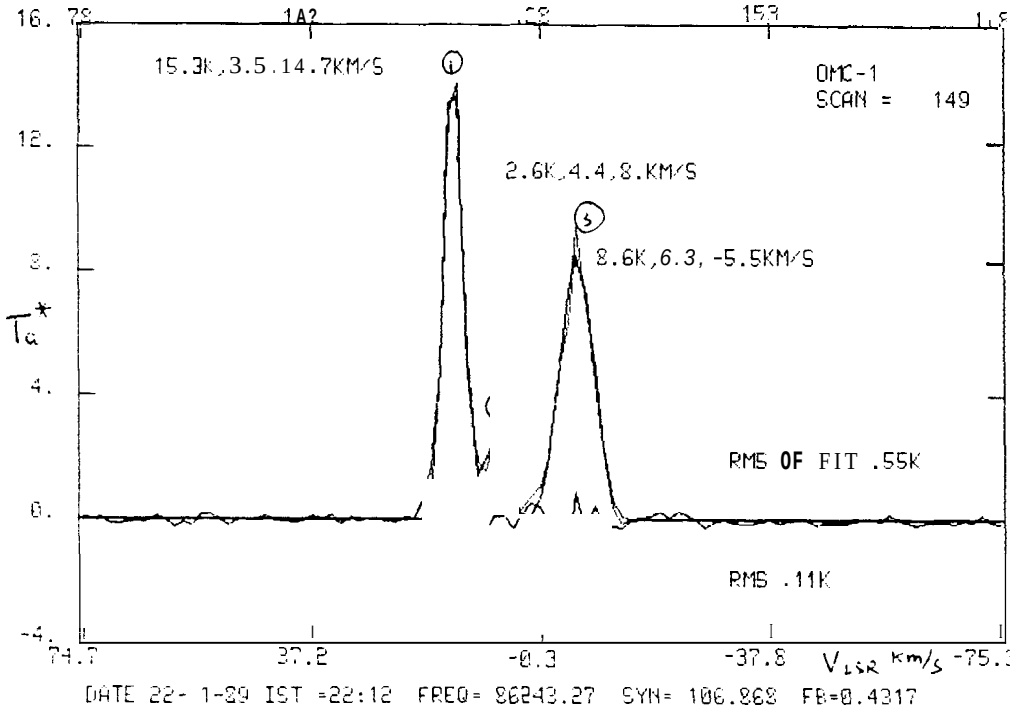

Figure 1: SiO maser emission from Orion A

Table 1: Orion calibration spectra. Gaussian-fitted parameters

		Ant.temp.(K)			Line-widths(km/s)			Velocities(km/s)		
No.	JD 244-	Ta_1^*	Ta_2^*	Ta_3^*	W_1	W_2	W_3	V_1	V_2	V_3
1	7206	7.50	2.00	9.40	3.60	9.60	6.60	15.90	10.90	-4.90
2	7208	6.80	2.40	9.40	3.20	11.80	6.40	16.20	13.70	-4.70
3	7218	7.80	2.40	9.80	3.00	11.90	6.70	15.40	11.50	-5.40
4	7218	6.90	1.90	7.80	4.10	8.80	6.70	16.10	9.90	-4.60
5	7233	7.25	1.50	7.50	4.10	6.40	7.20	14.90	8.00	-5.20
6	7236	7.30	1.60	7.70	4.00	6.90	6.40	16.70	10.00	-3.90
7	7238	8.70	1.40	8.30	3.00	10.90	5.60	15.60	10.00	-5.20
8	7238	8.10	1.80	8.50	4.00	6.10	6.60	14.90	9.30	-5.50
9	7263	6.90	1.30	7.30	4.30	5.90	6.50	15.00	8.60	-5.10
10	7265	6.60	1.80	7.00	4.00	6.20	6.10	15.00	9.00	-5.30
11	7271	9.00	2.30	10.00	3.90	7.50	6.10	16.90	10.20	-3.30
12	7541	14.20	2.30	9.00	3.60	5.00	5.70	15.90	9.10	-4.70
13	7548	15.30	2.60	8.60	3.50	4.40	6.30	14.70	8.00	-5.50
14	7551	14.30	2.30	8.00	3.60	4.70	6.40	15.30	8.70	-5.00
15	7552	16.80	2.60	8.90	3.40	4.40	6.30	15.60	8.90	-4.70
16	7983	15.90	3.70	6.90	3.00	1.60	6.30	15.50	8.80	-6.10
17	7984	17.00	3.00	6.90	3.90	3.20	6.70	15.40	8.40	-5.60

Table 1: (contd.) Errors on the parameters

No.	JD 244-	Antenna temp. (K)			Line-widths (km/s)			Velocities (km/s)		
		Ta_1^*	Ta_2^*	Ta_3^*	W_1	W_2	W_3	V_1	V_2	V_3
1	7206	0.26	0.16	0.19	0.15	0.89	0.16	0.07	0.27	0.08
2	7208	0.32	0.17	0.23	0.18	0.95	0.18	0.08	0.35	0.09
3	7218	0.38	0.19	0.26	0.17	1.11	0.20	0.09	0.43	0.09
4	7218	0.18	0.12	0.14	0.12	0.66	0.14	0.06	0.18	0.06
5	7233	0.13	0.11	0.10	0.09	0.53	0.11	0.05	0.13	0.06
6	7236	0.21	0.16	0.16	0.13	0.79	0.16	0.07	0.21	0.09
7	7238	0.43	0.22	0.31	0.17	2.02	0.24	0.10	0.48	0.10
8	7238	0.23	0.19	0.18	0.13	0.73	0.16	0.07	0.22	0.11
9	7263	0.19	0.16	0.15	0.13	0.64	0.16	0.07	0.17	0.09
10	7265	0.21	0.17	0.1	0.15	0.69	0.18	0.07	0.20	0.10
11	7271	0.22	0.16	0.18	0.11	0.61	0.13	0.05	0.23	0.09
12	7541	0.34	0.28	0.27	0.10	0.72	0.20	0.08	0.35	0.19
13	7548	0.36	0.32	0.27	0.10	0.63	0.23	0.10	0.36	0.21
14	7551	0.25	0.21	0.18	0.07	0.51	0.17	0.07	0.25	0.14
15	7552	0.33	0.29	0.24	0.08	0.56	0.20	0.08	0.34	0.20
16	7983	0.75	1.03	0.52	0.16	0.52	0.55	0.23	0.84	1.19
17	7984	0.99	1.09	0.76	0.26	1.35	0.85	0.36	0.97	0.87

Table 1. (contd.)

No.	JD 244-	σ	σ_{fit}	Area K km/s	Ratio Ta(1)/Ta(3)	bw/ch MHz	Area(1) K km/s	Area(3) K km/s
1	7206	0.24	0.38	116	0.80	0.49	3.09	4.77
2	7208	0.29	0.44	118	0.72	0.49	3.64	5.74
3	7218	0.51	0.51	130	0.80	0.49	4.27	6.69
4	7218	0.24	0.28	106	0.88	0.49	2.13	3.50
5	7233	0.17	0.19	100	0.97	0.59	1.87	2.47
6	7236	0.16	0.29	96	0.95	0.59	2.96	3.73
7	7238	0.26	0.79	95	1.05	0.25	3.26	7.03
8	7238	0.23	0.32	107	0.95	0.59	3.15	4.04
9	7263	0.17	0.27	90	0.95	0.59	2.63	3.41
10	7265	0.18	0.30	89	0.94	0.59	2.98	3.74
11	7271	0.29	0.31	123	0.90	0.59	3.02	4.01
12	7541	0.18	0.52	125	1.58	0.43	3.87	5.20
13	7548	0.11	0.55	130	1.78	0.43	4.15	5.49
14	7551	0.14	0.38	123	1.79	0.43	2.87	3.86
15	7552	0.18	0.49	136	1.89	0.43	3.72	4.87
16	7983	1.38	1.40	104	2.30	0.25	7.87	9.31
17	7984	0.37	2.10	135	2.46	0.25	9.46	15.71

of about 35%. Now we check how much of this is due to instrumental errors. The error on the integrated flux is related to the error in the antenna temperature as $\sqrt{N}\sigma\Delta V_o$, where ΔV_o is the resolution of the spectrometer and N is the number of channels within the profile. Assuming that the line-profile is described by a gaussian, the fractional error in integrated flux is related to the fractional error in the antenna temperature by

$$\frac{\Delta I}{I} = \frac{\sqrt{n}\Delta V_o}{1.06W}\frac{\Delta T}{T} \tag{5}$$

For each of the three gaussians we should then have $\frac{\Delta I}{I} = 0.5\frac{\Delta T}{T}$. Consequently, for the integrated flux over the whole profile (made of three gaussians having the same W), we would expect $\frac{\Delta I}{I} = 0.9\frac{\Delta T}{T}$. From Figs. 2 and 4, we see that $\frac{\Delta I}{I} \approx \frac{\Delta T}{T}$.

If the fluctuations in the antenna temperatures of these peaks are correlated, it is likely that there is an instrumental error(assumed to be constant over the bandwidth covered by the line-profile). In Fig. 6, we see that there is no correlation between the antenna temperatures of the two stronger peaks. However, Fig. 7 shows relative changes between peak (1) and peak **(3)** over a time scale of few tens of days (during the 1988 season). Therefore, a lack of correlation between the antenna temperatures of the two peaks does not straight away mean that the observation is free of (a common) calibration error. Moreover, the overall change in the integrated flux is seen to be significantly larger than the error bars given by $\sqrt{N}\sigma\Delta V_o$.

Before interpreting these as variations in the source itself, it is still necessary to consider the following cautions: What we have plotted is the antenna temperature which is corrected only for the atmospheric attenuation and telescope's ohmic losses by the chopper-wheel. The degradation of the aperture efficiency

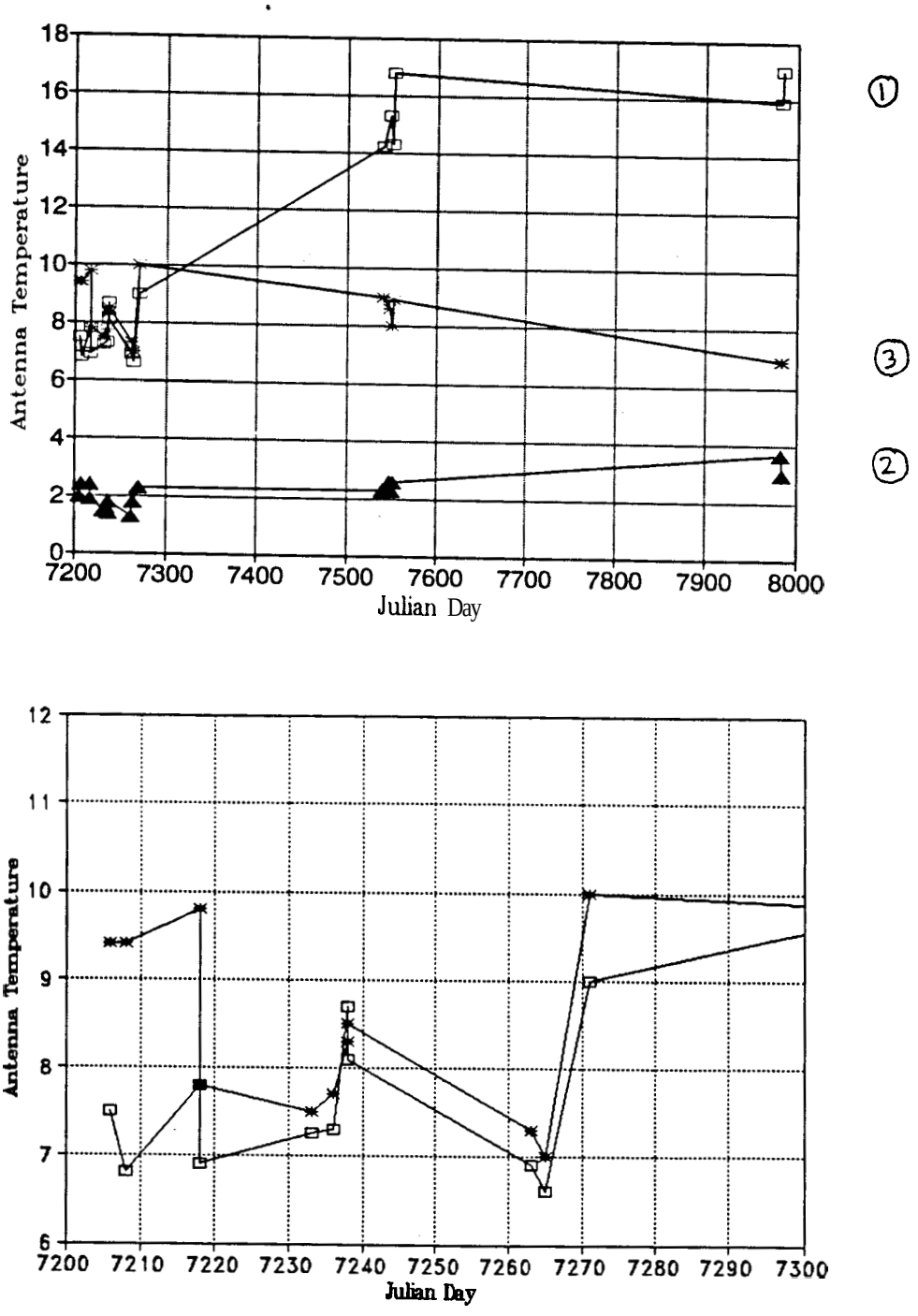

Figure **2:** Variation of antenna temperature from Orion

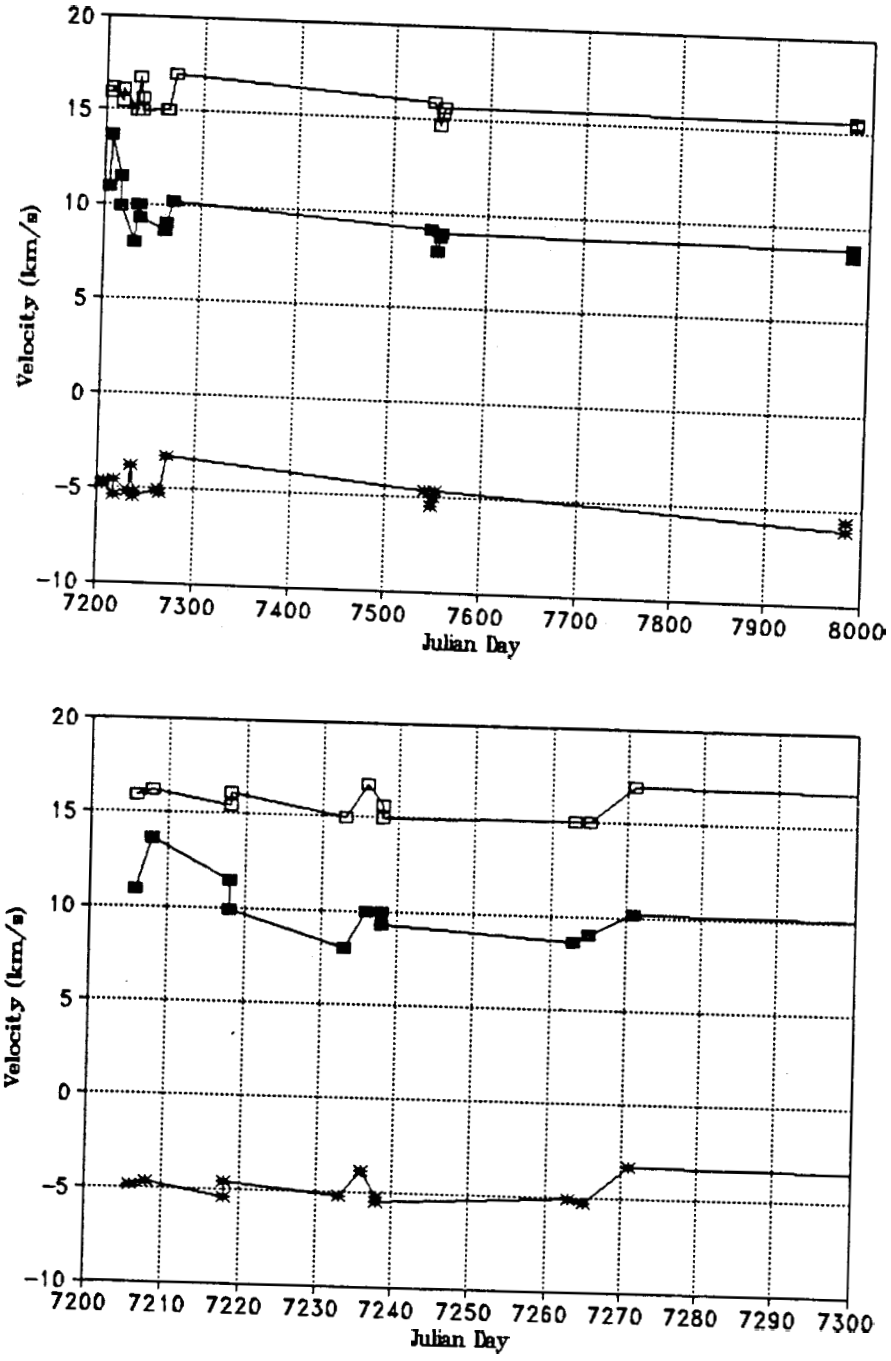

Figure 3: Orion: Variation of velocity

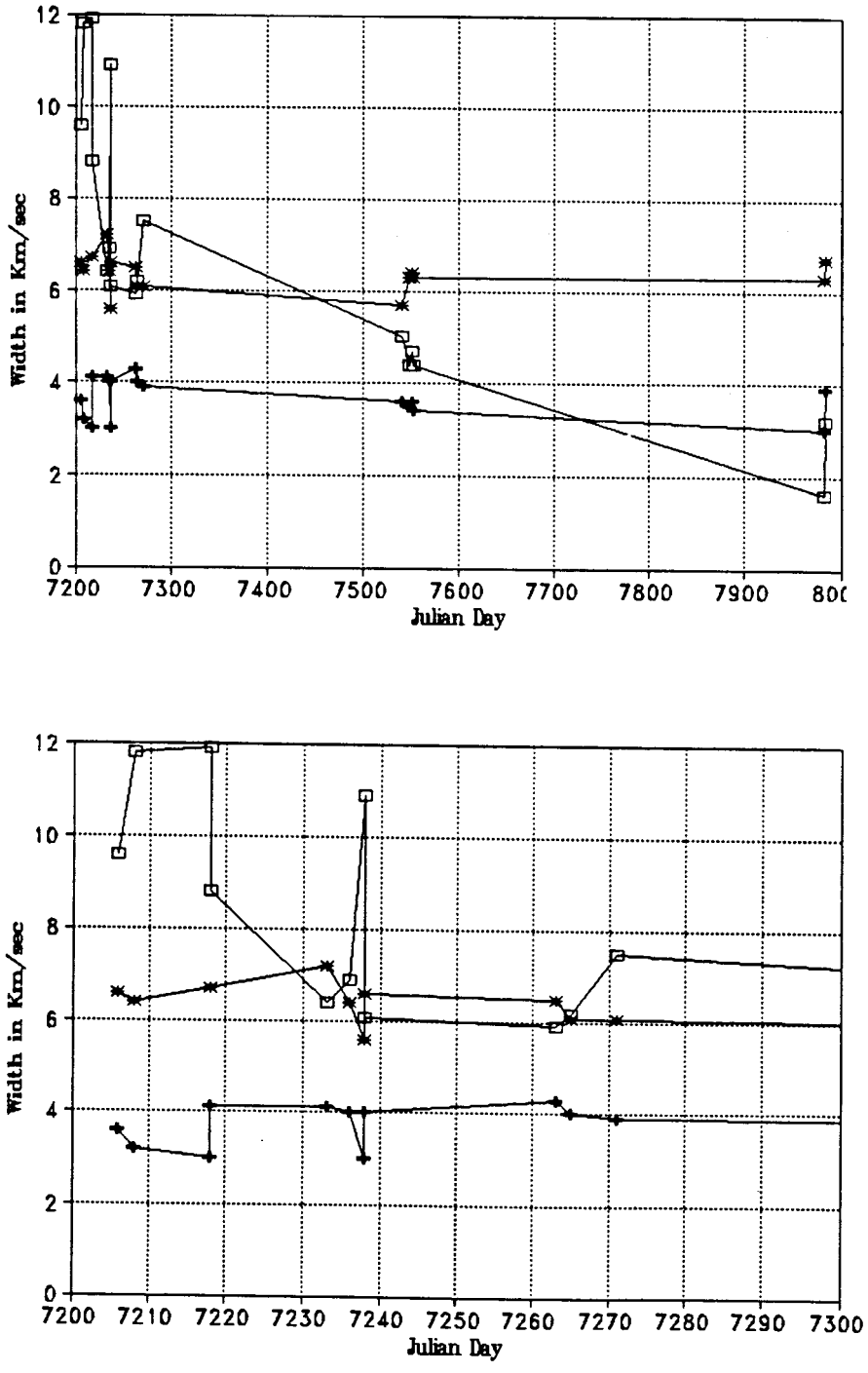

Figure 4: Orion: Variation of line-width

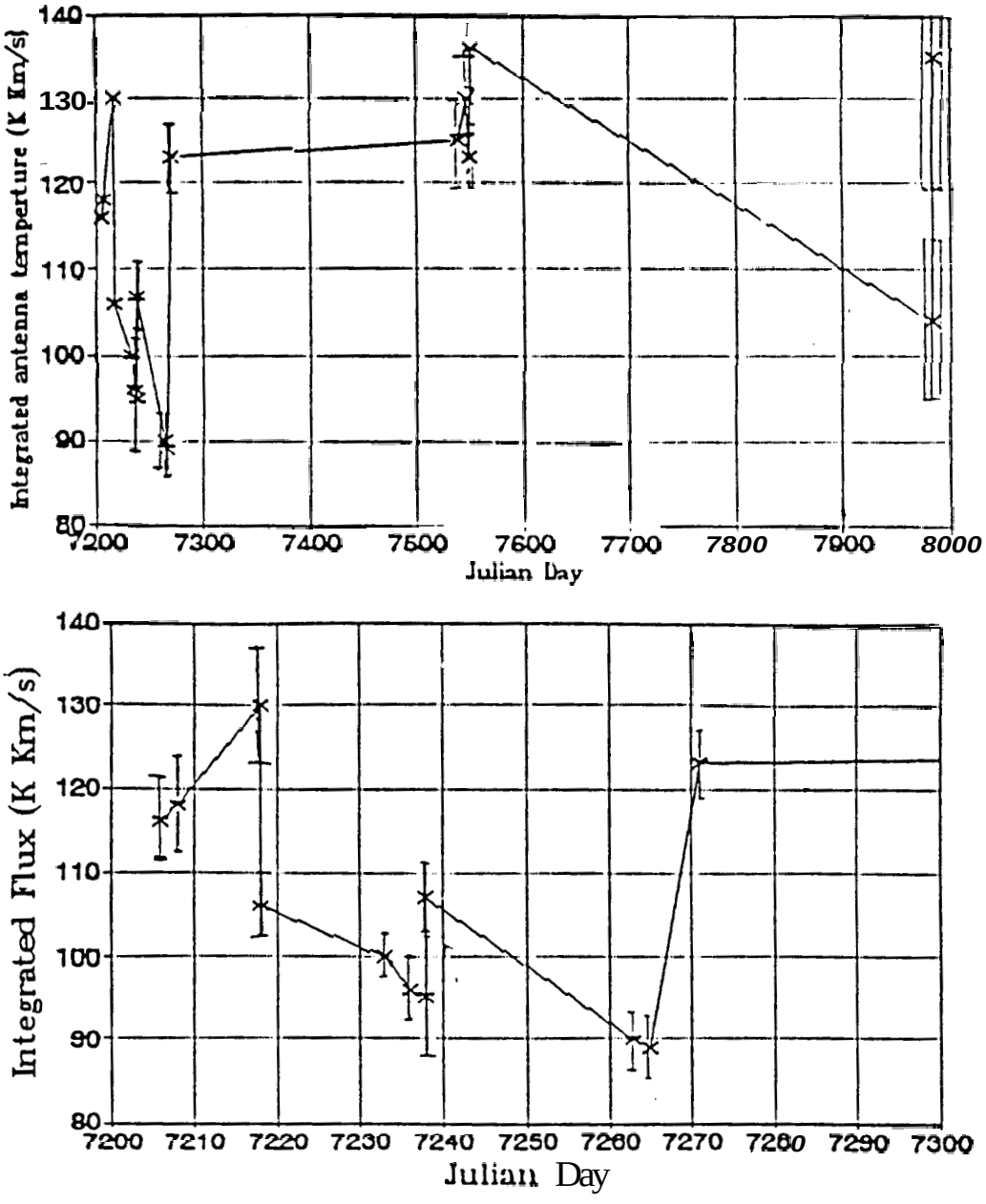

Figure 5: Orion: Variation of Integrated flux

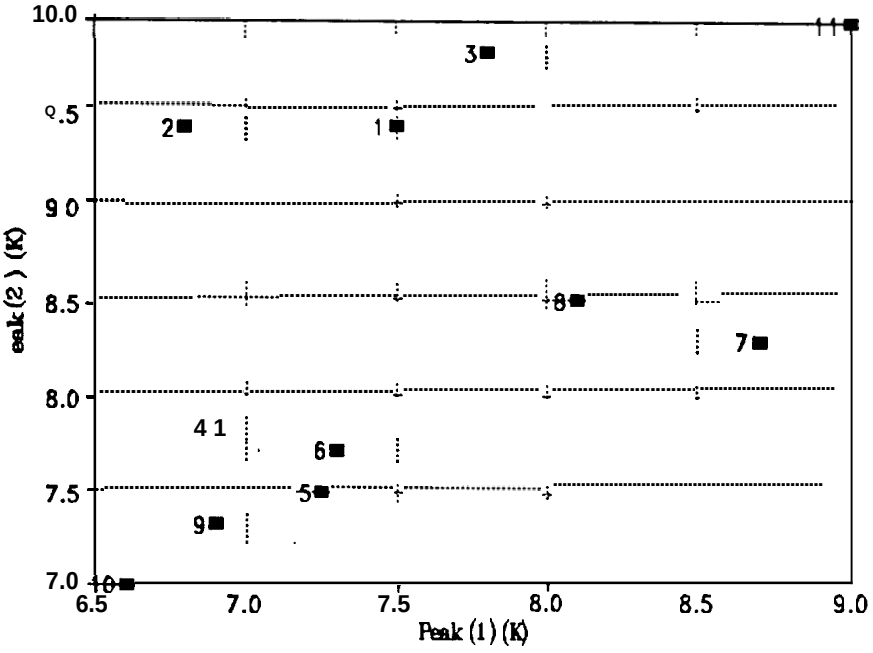

Figure 6: Orion: No correlation between the antenna temperatures of the two features

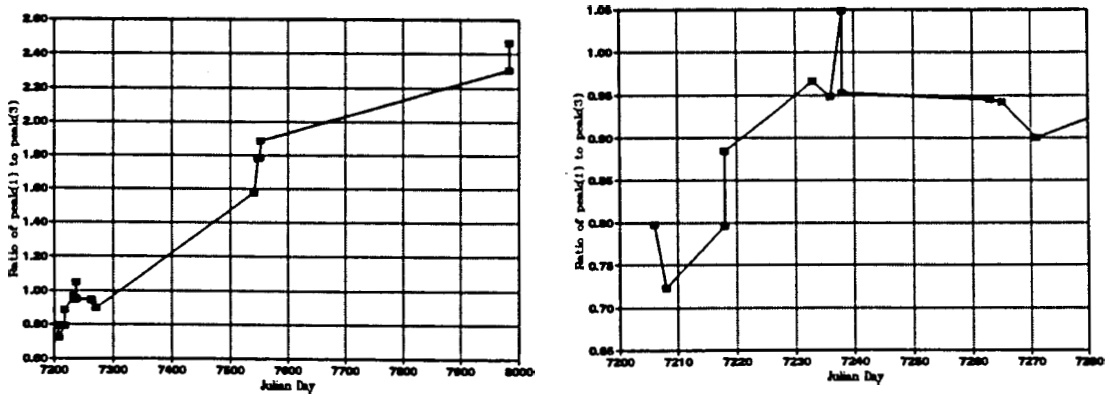

Figure 7: Orion: Variation of the ratio of the antenna temperatures of the two peaks

due to a distortion in the antennas response pattern either by heating of the dish due to the Sun, or by gravitational loading, may lead to a variation in the antenna temperature despite having a constant flux of radiation incident on the telescope. In Fig. 8—10 we have plotted the integrated flux against elevation, time and the polarization parallactic angle. There is some indication in Fig 9, of a dependence of the gain on the time of observation. All the points observed between 15hrs and 20hrs are significantly lower. However, most of the SiO sources were observed during the night, except in the 1990 season when there were a substantial number of sources observed during afternoons, for which this drop in the aperture efficiency is taken into account (in the next Chapter).

To summarize, during 1988 we have a maximum calibration error of about 20%. (Corroborated by Jupiter measurements). The variations larger than this amount seem to be inherent time variations in the source. It is interesting to note that Martinez et al. (1989), in their time-monitoring of Orion, also find variations of the same order over similar time-scales. As we shall see from the Jupiter scans, the overall calibration error during 1989 and 1990 is not more than 10 to 15%. We believe that the difference in the 1988 observations arises due to the fact that we did not have the chopper-calibration as often as in the 1989 and 1990 seasons. In the latter seasons, we took the chopper runs nearly every 100 seconds during the spectral-line observations. This was made possible by putting the chopper/mirror under computer control.

3.3 Jupiter Scans

Since the scans were taken in elevation after correcting for the pointing error in azimuth, the peak flux on the scan is free of pointing errors. The errors on the

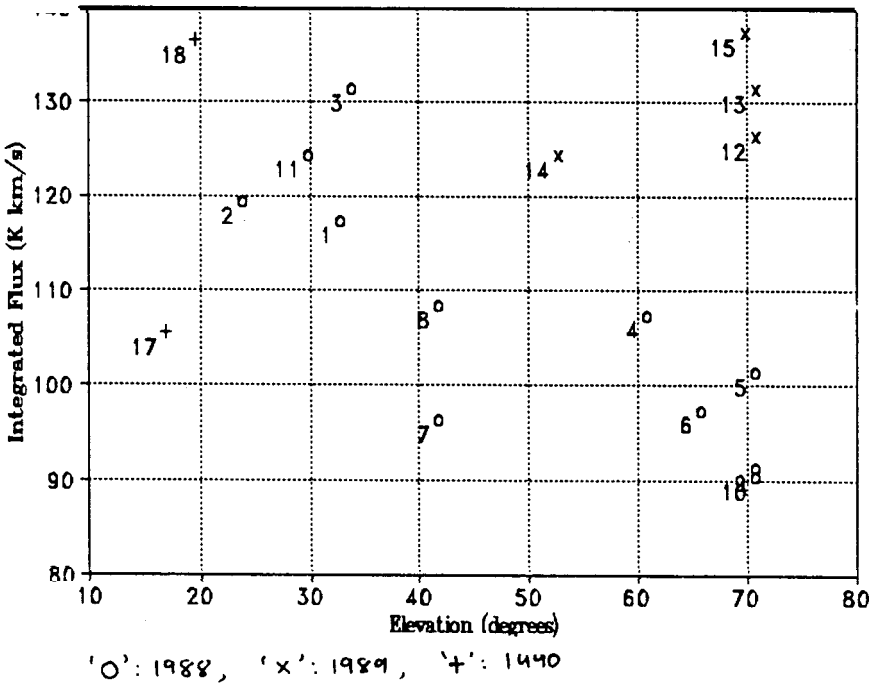

Figure 8: Integrated flux from Orion in different years, as a function of elevation

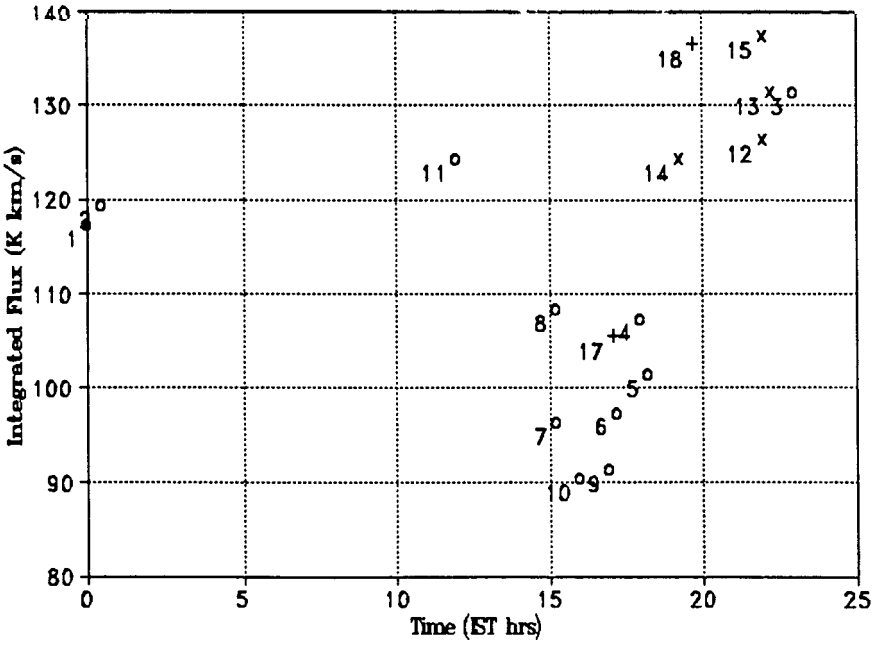

Figure 9: Same as Fig. 8, as a function of time (IST)

parameters obtained from these scans therefore are due to either the inherent system noise and/or an error in the correction for the atmospheric attenuation. The scans typically have a S/N of greater than 15 so the error due to inherent noise is negligible. The correction for atmospheric attenuation is done using a chopper-wheel. During 1988 we had used a teflon sheet of thickness about 1mm, as the chopper. The advantage of this over a regular absorber is that it gives a smaller step in voltage on chopper switching, of the same order as obtained from switching between a source and the sky; which is desirable to ensure that the backends operate in a linear range. The aperture efficiency obtained during the three observing seasons are presented in Table 2. Plots of these are shown as a function of elevation and time, in Figs. 11—19. In 1988 we have a peak-to-peak variation of aperture efficiency of by about 20%. Within these limits there does not seem to be any systematic dependence on either elevation or time. The 1989 observations of Jupiter and Venus show a smaller mean value of efficiency but there is less scatter in it. There are two factors which are different in these two sets of measurements.

During 1988, all scans on planets were taken on a chart-recorder, with manual control of the chopper and the mirror. During 1989, the scans were taken by recording the total power voltage through an A/D and later fitting gaussians to them to obtain the peak flux, pointing offsets, convolved beam-width, etc. In addition, the chopper and mirror control was under computer-control minimising the loss of time between the chopper cal runs and the scan. These two factors lead to a greater accuracy in measurements after the 1988 season. The SiO observations during 1989, were interrupted by a malfunction in the cryogenics (in the cold-head). The cold-head was replaced in the 1st week of March 1989

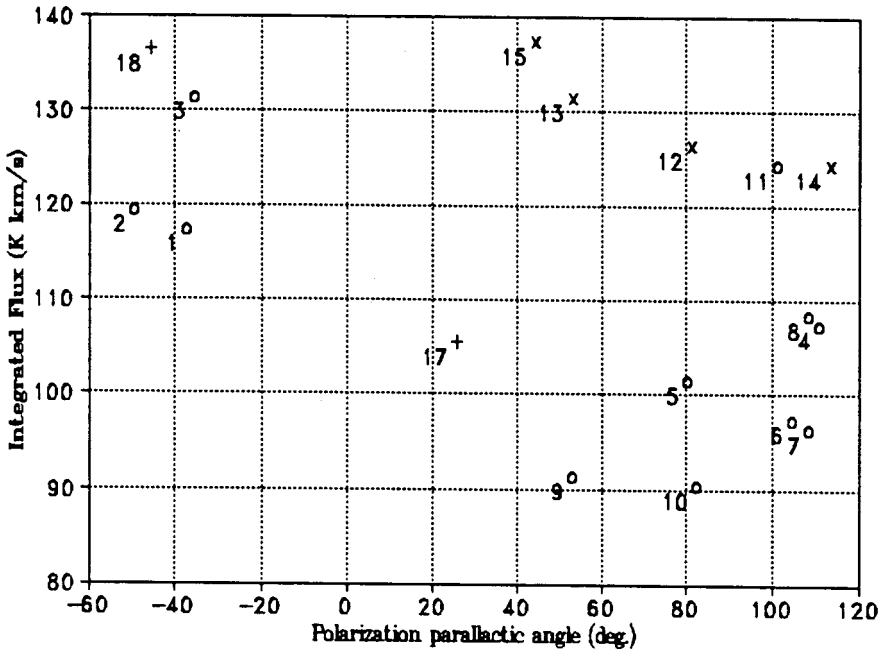

Figure 10: Same as Fig. 8, as a function of Polarization parallactic angle

Table 2: Aperture efficiency (1988)

Date	Elevation	$\eta\%$	η^a	Time(IST hrs)	Source
11-2-88	66.75	45		18.00	Jupiter
11-2-88	46.10	45		19.47	Jupiter
11-2-88	37.88	40		19.95	Jupiter
11-2-88	35.00	44		20.22	Jupiter
11-2-88	20.35	34		21.25	Jupiter
16-5-88	26.00	49	48.5	16.07	Jupiter
16-5-88	24.00	44	43.5	16.18	Jupiter
16-5-88	58.00	39	38.5	16.75	Venus
16-5-88	55.00	40	39.5	17.02	Venus
16-5-88	46.00	47	46.5	17.65	Venus
16-5-88	43.00	50	49.5	17.87	Venus
16-5-88	35.00	54	53.5	18.45	Venus
16-5-88	26.00	48	47	19.15	Venus
18-5-88	36.37	49		18.32	Venus
19-5-88	57.05	50		12.33	Venus
19-5-88	59.58	49		12.62	Venus
19-5-88	74.30	48		13.75	Venus
19-5-88	175.00	46		13.92	Venus

[a] These values were obtained on using a hot-load instead of the teflon chopper. This shows that the difference is insignificant

Table 2. (continued) 1989

No.	Date Feb'89	Time	El.	Scan Dia (")	Jupiter Dia (")	Beam Dia (")	Ta^* (K)	σ (K)	η
1	8	21.17	53.95	81	39.68	73.55	12.1	0.05	0.37
2	8	21.42	50.57	80	39.68	69.47	11.7	0.04	0.36
3	8	21.63	47.57	81	39.68	70.62	11.8	0.03	0.37
4	8	21.9	43.88	78	39.68	67.16	11.7	0.03	0.37
5	8	22.15	40.18	80	39.68	69.47	11.6	0.03	0.36
6	8	17.22	70.93	84	39.15	74.32	11.9	0.03	0.38
7	12	17.6	75.98	86	39.15	76.57	11.9	0.04	0.37
	12	20.77	56.68	83	39.15	73.19	12	0.04	0.38
	12	21.52	45.92	82	39.15	72.05	12	0.04	0.38
	12	21.95	38.97	84	39.15	74.32	11.5	0.03	0.36
	12	22.3	35	84	39.15	73.83	11.6		0.37
12	12	22.38	33.67	84	39.15	73.83	11.4		0.36

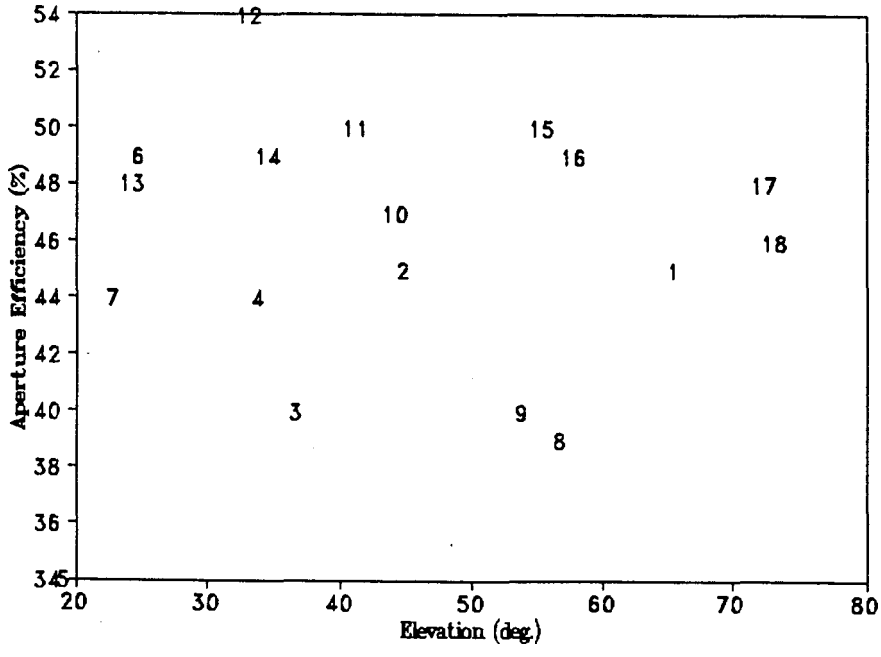

Figure 11: Aperture efficiency as a function of elevation during 1988

Table 2: (continued] 1990

No	EL deg.	IST hrs	Beam Dia (")	Ta* (K)	Baseline DC (K)	σ (K)	η
1	34.75	18.58	76.3	15.5	-7.1	0.81	0.38
2	42.62	19.13	74.6	14.4	-6.1	0.74	0.36
3	47.59	19.48	80.4	12.5	-5.4	0.65	0.31
4	49.22	19.60	77.6	13.2	-5.1	0.77	0.33
5	50.83	19.72	80.6	13.3	-4.9	0.62	0.33
6	52.55	19.83	78.6	13.8	-4.4	0.65	0.34
7	56.00	20.08	79.4	13.4	-3.8	0.64	0.33
8	67.13	20.88	87.5	13.1	-2.6	0.7	0.32
9	73.63	21.40	85.8	12.3	-2.3	0.61	0.30
10	78.05	21.85	92.9	12.4	-2.2	0.68	0.30
11	79.18	22.03	90.3	12.2	-2	0.52	0.29
12	79.82	22.22	93.6	12.1	-2.2	0.53	0.29
13	77.80	22.75	92.6	12.4	-2.2	0.67	0.30
14	74.46	23.47	94.7	12.5	-2.4	0.62	0.30
15	72.47	23.63	93.3	12.5	-2.5	0.64	0.30
16	70.12	23.82	89.6	12.6	-2.4	0.58	0.30
17	67.59	24.02	85.4	12.7	-2.3	0.7	0.31
18	57.39	24.75	71.6	13.6	-2.9	0.98	0.34
19	50.79	25.23	78.4	14.2	-4	0.76	0.35
20	47.76	25.45	95.9	14.4	-4.7	1.1	0.34
21	46.23	25.57	77.1	14.3	-4.2	0.91	0.35
22	37.40	26.18	79.4	16.4	-6.3	0.83	0.40
23	34.26	26.40	72.2	16	-6.6	0.65	0.40
24	30.86	26.63	74.6	16.1	-6.9	0.65	0.40
25	27.50	26.87	73.3	16.4	-7	0.69	0.41
26	24.76	27.07	74.6	16.2	-7	0.8	0.40
27	22.99	27.18	72.6	15.8	-7	0.73	0.40
28	20.56	27.35	68.2	15.9	-7.1	0.7	0.41
29	18.87	27.47	77.0	15.6	-7.1	0.64	0.39

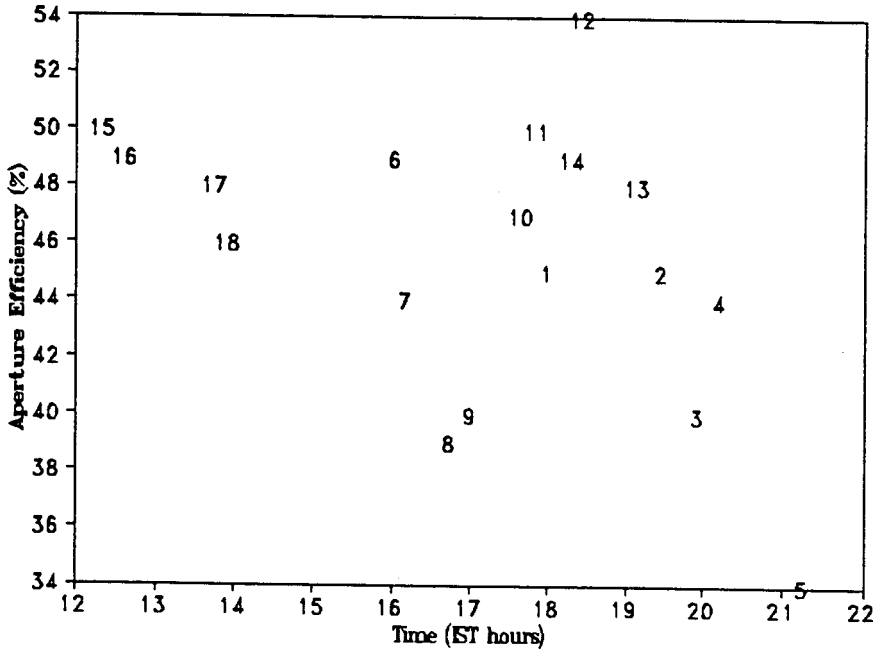

Figure 12: Aperture efficiency as a function of time (IST), (1938)

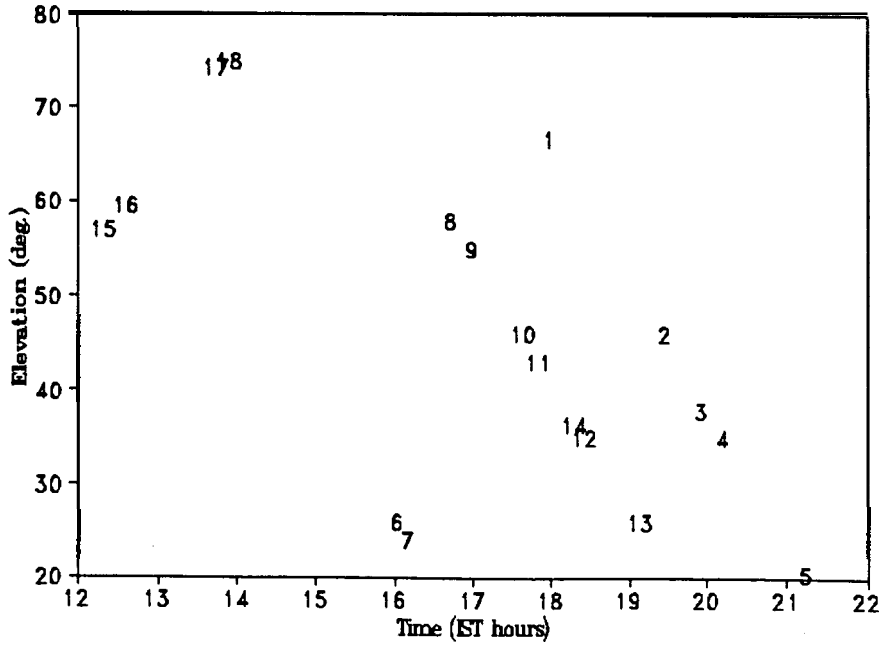

Figure 13: Elevation of Jupiter as a function of time. This Fig. helps separating the dependences on elevation and time seen in Figs. 11 and 12

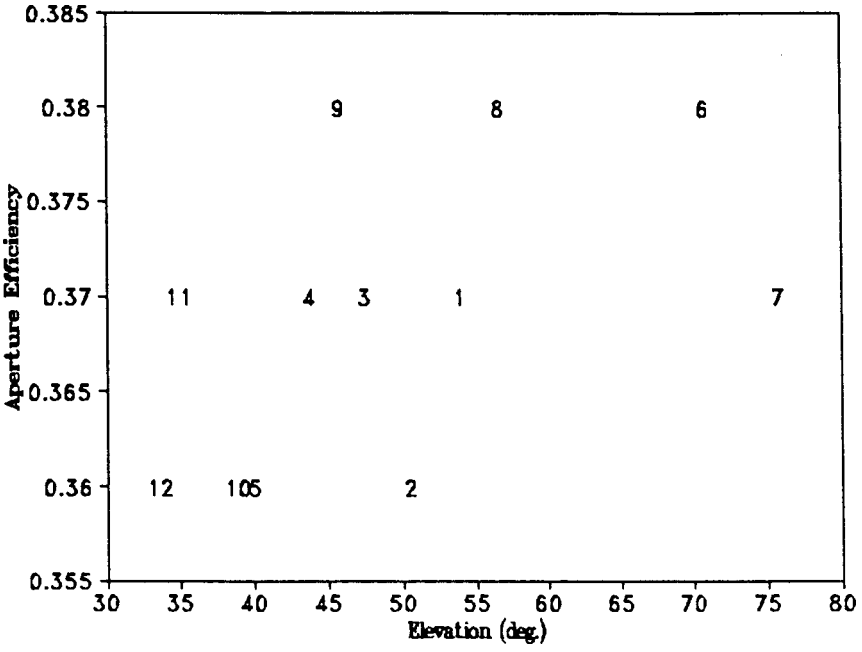

Figure 14: Same as Fig. 11, for 1989

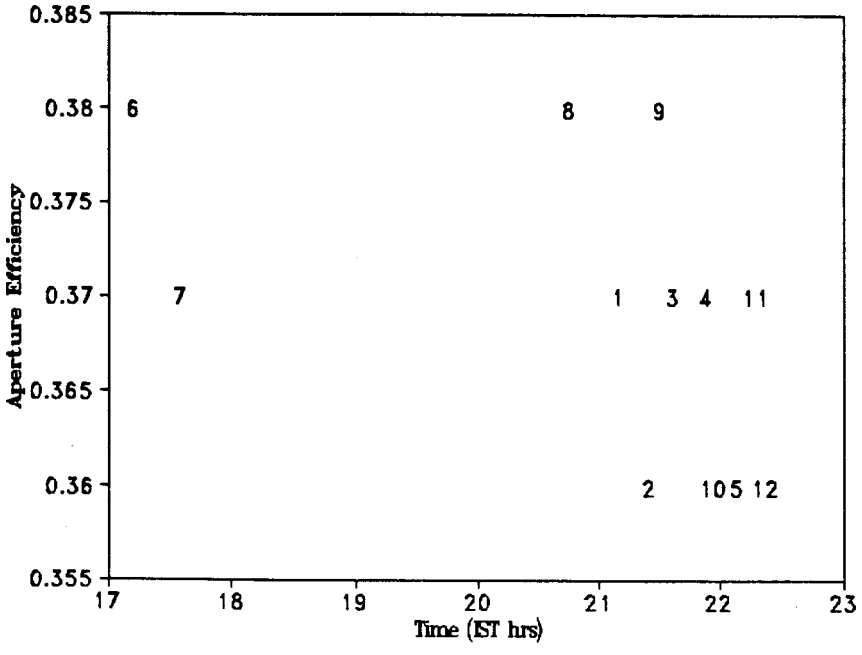

Figure 15: Same as Fig. 12, for 1989

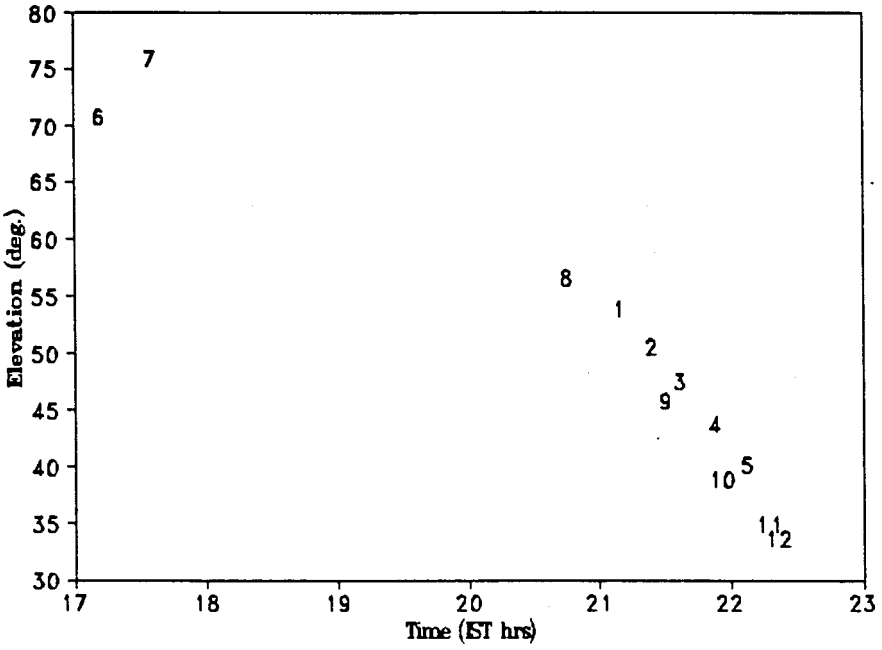

Figure 16: Same as Fig. 13, for 1989

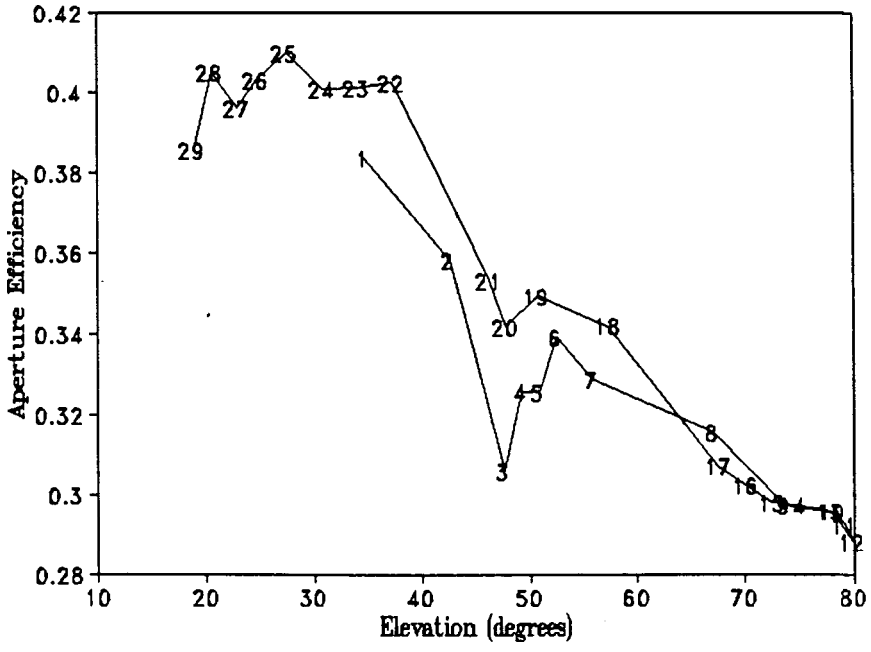

Figure 17: Same as Fig. 11, for 1990

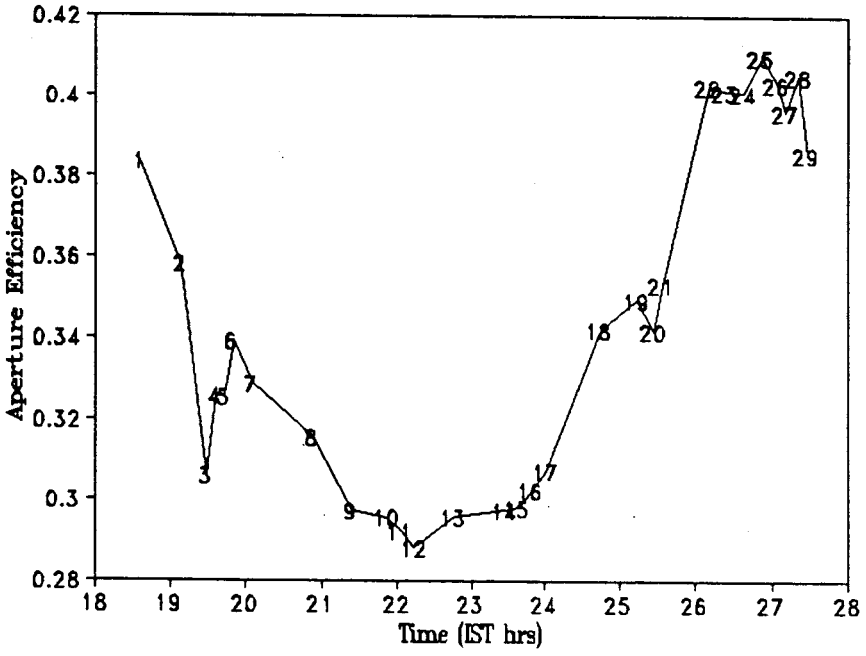

Figure 18: **Same** as Fig. 12, for 1990

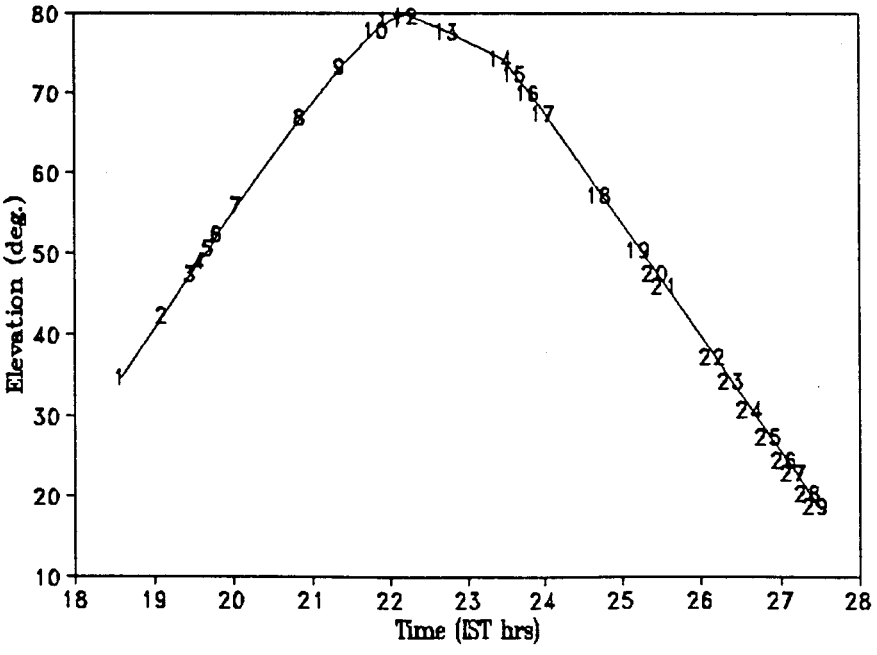

Figure 19: Same as Fig. 13, for 1990

and the feed inside the dewar was re-aligned. All the scans taken after this time, show a very systematic dependence of aperture efficiency with respect to elevation, including the scans taken during 1990. This behaviour is shown in Fig. 20. The fitted curve is used to correct the fluxes in observations of SiO masers made at different elevations during the 1990 season (in the next Chapter). In this figure we also see that the residuals are not dependent on time between 18 to 4 hrs. IST.

3.4 Check runs on R Cas

The observations of R Cas were made in the frequency switching mode. The line-profile shows two prominent narrow features. The variation of integrated flux is shown in Fig. 21. This is the expected variation according to the noise in the baseline. This puts an upper limit on the calibration error due to mirror/chopper switching, to be about 25%. (On the other hand, we know that from successive scans taken on planets, the variation in the measured flux is not more than 10 to 15%.)

The variation of the antenna temperatures of the peaks (Fig. 21) however, is complicated by the fact that the two features seem to have different linear polarizations with respect to each other (Fig. 22). The ratio of antenna temperatures of these two spikes is independent of calibration errors, and is shown in Fig. 23, as a function of time and in Fig. 24, as a function of the polarization parallactic angle. Once again we check (in Fig. 25), for a correlation between the antenna temperatures of the two peaks. If there had been one, it would have indicated a possible instrumental calibration error (common to both the spikes) but none is seen.

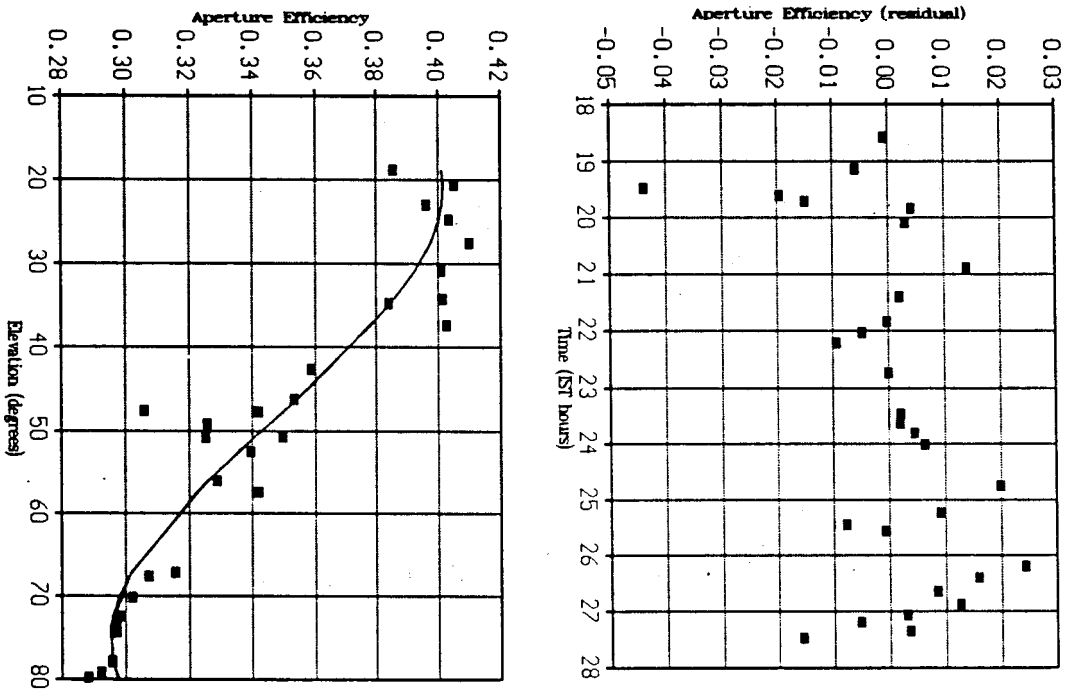

Figure 20: Aperture efficiency as a function of elevation, during 1990. The fitted curve was used for correcting the observed fluxes

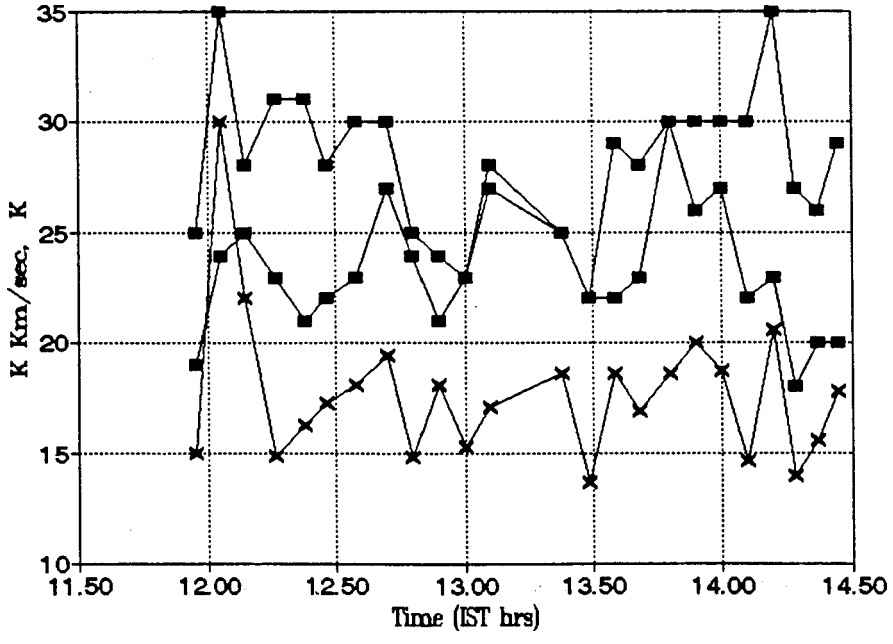

Figure 21: Variation of Integrated flux and antenna temperature from R Cas over a period of about 2 hrs

Observations of polarization in R Cas have been reported before by Clark et al. (1982) and McIntosh et al. 1989. Comparing our observations with the latter, there appears a systematic change in the relative polarizations of the two main features in the profile from R Cas. More time-monitoring observations of polarization are needed however, for reliable interpretations.

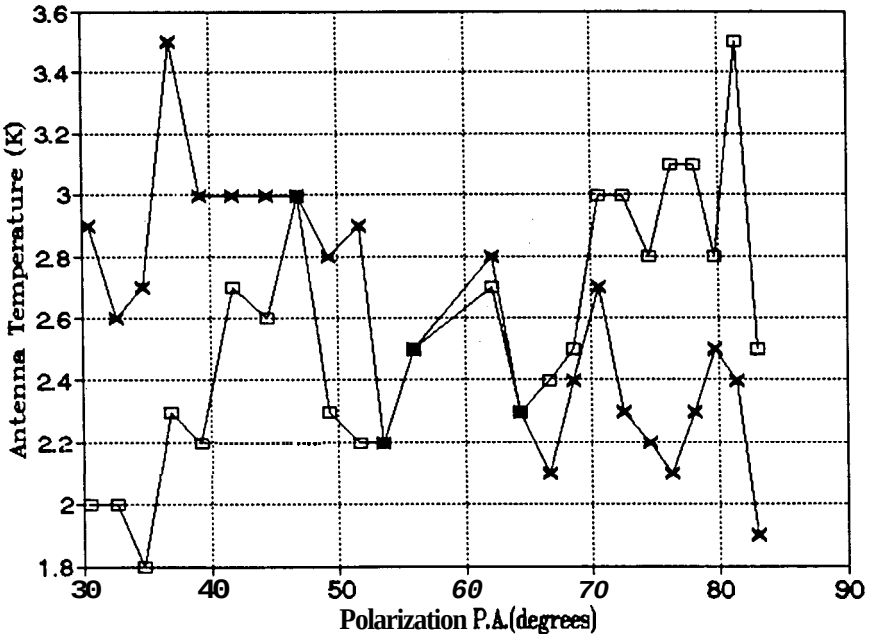

Figure 22: Antenna temperature from R Cas, as a function of polarization parallactic angle

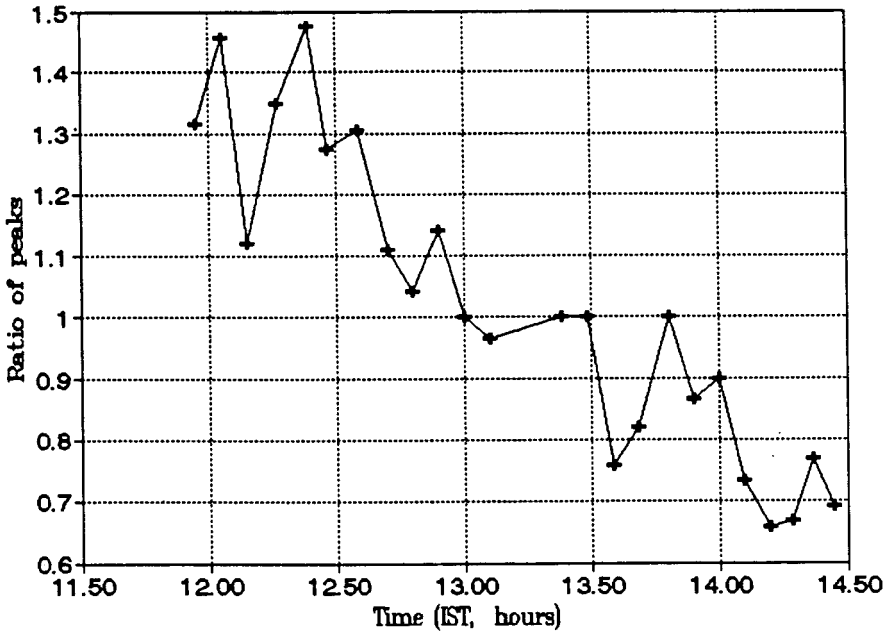

Figure 23: Ratio of antenna temperatures of the two features in R Cas as function of time

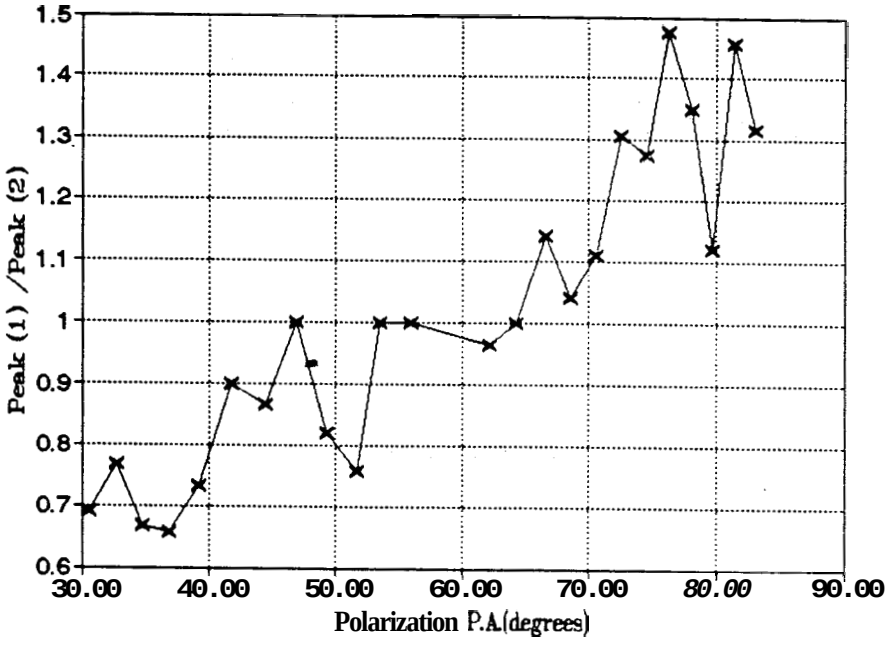

Figure 24: Same as Fig. 23, as a function of polarization parallactic angle

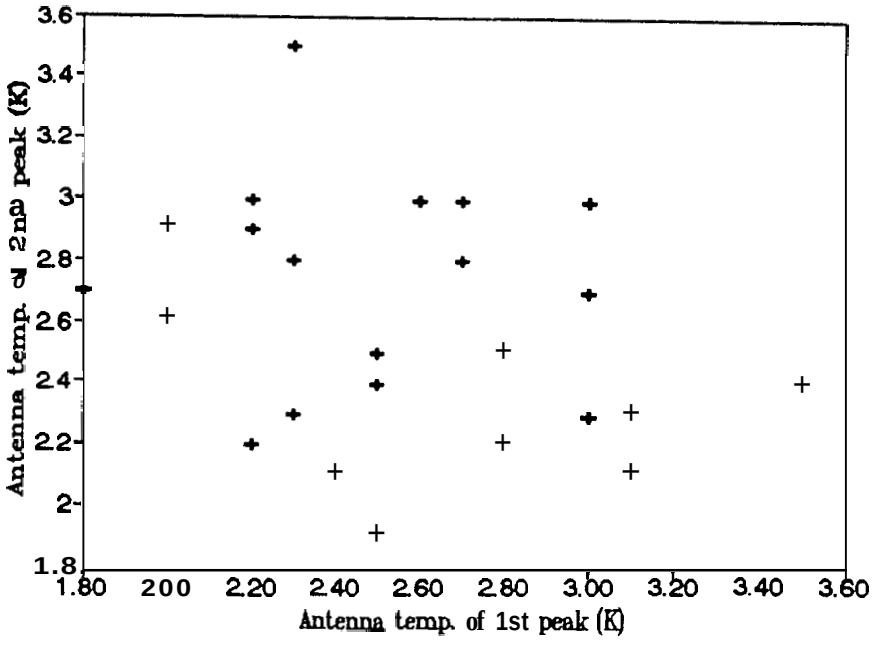

Figure *25:* Checking for correlation between the antenna temperatures of the two features in R Cas

REFERENCES

Martinez A., Bujarrablal V., Alcolea J., 1988, *Astron. Astrophys. Supp. Ser.* 74,273.

McIntosh G. C.,et al., 1989, *Ap. J.* 337,934.

Alien B.,1984 Ph.D. Thesis, MIT.

Wilson R. W., Jefferts K. B., Penzias A. *A.,* 1971, *Ap. J.* **161**,L43.

Woolf N. J., Ney E. P., 1969, *Ap. J. Lett.* **155**,L181.

Wright *M.* C. H., et al., 1990, *Astron. J.* 99,1299.

Clark F. O., Troland T. H., Johnson D. R., 1982, *Ap. J.* 261,569.

Rieu N. Q., 1969, *Astron. Astrophys.* 1,128.